

Solitons and nonlinear waves along quantum vortex filaments under the low-temperature two-dimensional local induction approximation

Robert A. Van Gorder
*Mathematical Institute, University of Oxford,
Andrew Wiles Building,
Radcliffe Observatory Quarter, Woodstock Road,
Oxford, OX2 6GG, United Kingdom
Robert.VanGorder@maths.ox.ac.uk*

Very recent experimental work has demonstrated the existence of Kelvin waves along quantized vortex filaments in superfluid Helium. The possible configurations and motions of such filaments is of great physical interest, and Svistunov previously obtained a Hamiltonian formulation for the dynamics of quantum vortex filaments in the low-temperature limit under the assumption that the vortex filament is essentially aligned along one axis, resulting in a two-dimensional problem. It is standard to approximate the dynamics of thin filaments by employing the local induction approximation (LIA), and we show that by putting the two-dimensional LIA into correspondence with the first equation in the integrable Wadati-Konno-Ichikawa-Schimizu (WKIS) hierarchy, we immediately obtain solutions to the two-dimensional LIA, such as helix, planar, and self-similar solutions. These solutions are obtained in a rather direct manner from the WKIS equation, and then mapped into the 2D-LIA framework. Furthermore, the approach can be coupled to existing inverse scattering transform (IST) results from the literature, in order to obtain solitary wave solutions including the analogue of the Hasimoto 1-soliton for the 2D-LIA. One large benefit of the approach is that the correspondence between the 2D-LIA and the WKIS allows us to systematically obtain vortex filament solutions directly in the Cartesian coordinate frame without the need to solve back from curvature and torsion. Implications of the results for the physics of experimentally studied solitary waves, Kelvin waves, and post vortex reconnection events are mentioned.

PACS numbers: 05.45.Yv, 67.30.he, 47.32.C-

I. INTRODUCTION

The study of vortex filament dynamics in quantum fluids has been of great interest in recent times, as quantized vortex filaments have been experimentally observed in superfluid Helium. Due to the low viscosity of superfluid Helium, such quantized vortex filaments can persist at larger timescales than their classical vortex filament counterparts, making such filament solutions realizable in experiments. Furthermore, vortex filament tangles and vortex reconnection events have been seen as harbingers of quantum turbulence, and indeed such vortex dynamics have been shown to degenerate into turbulence in a number of numerical simulations. Therefore, the construction of vortex filament solutions in the low temperature regime is of great interest both physically and mathematically.

In this paper, we shall employ an integrable systems approach in order to study the dynamics of vortex filaments under a localized form of a specific model derived by Svistunov [1, 2]. For many scenarios, particularly when the vortex filaments are not too tightly coiled or do not self-intersect, such local models give us an accurate understanding of the temporal dynamics of the vortex filaments. Physically, present results allow us to obtain physically interesting solutions for the dynamics of vortex filaments in the very low temperature regime of superfluid Helium. As we shall discuss later, a number of the analytical solutions obtained here correspond nicely to prior numerical simulations or experimental work. Yet, by virtue of studying these dynamics through an integrable systems approach, we obtain a coherent and organized treatment of such solutions. Mathematically, the results demonstrate the utility of the map between the two-dimensional local induction approximation (2D-LIA) and the first equation in the Wadati-Konno-Ichikawa-Schimizu (WKIS) hierarchy. Furthermore, and somewhat importantly, the 2D-LIA can be used to obtain vortex filament solutions in the Cartesian coordinate frame directly. In contrast, using the connection between the nonlinear Schrödinger equation (NLS) and standard local induction approximation (LIA), one would obtain solutions in terms of the curvature and torsion of the vortex filament. Then, one would need to integrate the Frenet-Serret formulas in order to recover the tangent vector to the filament. This tangent vector would then need to be integrated in order to recover the explicit Cartesian representation for the vortex filament curve. Therefore, the present approach is more computationally efficient for those filaments we construct. As such, while connections between the NLS, WKIS, and standard LIA have been considered before, the present connection to the 2D-LIA allows us to obtain Cartesian representations of the vortex filaments in a direct manner worth exploring.

To begin with, recall that in the very low temperature regime, the self-induced dynamics of a thin vortex filament

are given by the Biot-Savart formulation [1–3]

$$\mathbf{r}_t = \frac{\Gamma}{4\pi} \int \frac{(\mathbf{s} - \mathbf{r}) \times d\mathbf{s}}{|\mathbf{s} - \mathbf{r}|^3}. \quad (1)$$

The integration is over the length of the filament \mathbf{r} , and Γ represents the strength or circulation of the filament. The non-local dynamics are often approximated by the local induction approximation (LIA), which gives [4, 5]

$$\mathbf{r}_t = \gamma \kappa \mathbf{t} \times \mathbf{n}, \quad (2)$$

where κ is curvature, \mathbf{t} is the tangent vector to the curve, \mathbf{n} is the normal vector to the curve, and $\gamma = \frac{\Gamma}{4\pi} \ln\left(\frac{\ell}{a}\right)$, where $a > 0$ denotes the vortex filament radius and ℓ denotes the inter-vortex distance. This formulation introduces a cutoff at $a < |\mathbf{r} - \mathbf{s}|$ to avoid the singularity in (1). The well-known Hasimoto transformation [6] can be used to map (2) directly into the cubic NLS equation, with the resulting complex scalar potential encoding the curvature and torsion of the filament. This approach has been used in a number of works, where one obtains a particular solution to the cubic NLS equation and inverts the Hasimoto map in order to obtain a vortex filament solution to the LIA. Solutions such as one-solitons [6], N -solitons [7], breathers [8, 9], multiple breathers [10], and torus knots [11] have been found via such an approach. Some of these theoretical results were even demonstrated to be experimentally relevant [12–14]. Furthermore, the relation between an extended Wadati-Konno-Ichikawa (WKI) model (which includes a sign term) and the LIA has been explored [15], and both one-soliton [16, 17] and multi-soliton [18] solutions have been obtained. Therefore, there is an obvious connection between the LIA (2), the cubic NLS, and members of the integrable WKIS hierarchy. This motivates us to obtain similar results for the so-called 2D-LIA [1] derived from a 2D-Biot-Savart integral by [2]. Since solutions are known already for the standard 3D form of the LIA, one may wonder why we wish to directly consider solutions of this 2D-LIA. One primary benefit is that the 2D-LIA employed is derived in Cartesian coordinates, and hence once we have a solution, we immediately know the vortex filament curve. Meanwhile, for the solutions resulting from the connection between the 3D LIA and the cubic NLS equation, note that the solutions are obtained for the curvature and torsion of the filament curve and given in terms of a parameterization of arclength. While these quantities are useful for understanding qualitative features of the solution curves, one must then invert the Frenet-Serret formulas in order to recover the actual vortex filament curve in Euclidean space. Therefore, the solutions under 2D-LIA allow us to directly see the filament curves, provided that certain conditions hold which permit uniquely defined filament curves. We outline specific mathematical requirements in the next section.

The 2D-LIA can be derived from Svistunov’s Hamiltonian formulation [2] for the dynamics of a thin vortex filament in the very cold superfluid limit, and this was done in [1]. The benefit of this model is that it permits one to recover the extrinsic form of the vortex filament in Cartesian coordinates, assuming that the vortex filament is aligned along one axis and is of sufficiently bounded variation. The drawback is that, by expressing the vortex filament in extrinsic form, the mathematical model is more complicated than the standard LIA in the intrinsic space (where the solution is expressed in terms of curvature and torsion). The goal of the present paper will be to obtain a result similar to that of the Hasimoto transformation, and then exploit that transformation in order to recover vortex filament solutions. While the standard LIA can be put into correspondence with the cubic NLS equation and also with the extended WKIS model, we show that the 2D-LIA can be put into correspondence with the first equation of the integrable WKIS hierarchy [19, 20]. Therefore, while the 2D-LIA is derived differently than the standard LIA, both equations are integrable and one may search for their respective vortex filament solutions by solving simpler integrable models.

In Sec. II, we shall follow Svistunov’s Hamiltonian formulation for the dynamics of a thin vortex filament in the very cold superfluid limit in which mutual friction effects are negligible, and arrive at the 2D-LIA derived by [1]. However, we then show that the resulting 2D-LIA can be put into correspondence with one of the WKIS equations, in particular, the first equation of the WKIS hierarchy. The utility of this approach lies in the fact that the WKIS model is simpler than the 2D-LIA (since the 2D-LIA involves derivatives of the unknown potential function in a nonlinear term), while both equations are still far more complicated than the cubic NLS. Since solutions of the WKIS are known via the inverse scattering transform, this effectively allows us to use such results to recover vortex filament solutions to the 2D-LIA. In Sec. III, we give the most general form of stationary solutions for the WKIS model, before transforming these into solutions of the 2D-LIA. These solutions are related back to those of [21, 22] which were obtained directly from the 2D-LIA. We find that the solutions more readily come out of the WKIS framework. As special cases, one can recover planar and helical filament structures. In Sec. IV, we obtain self-similar solutions to the WKIS model (which have not been previously considered in the literature) and we use these to construct self-similar solutions to the 2D-LIA. The solutions are in agreement with those discussed previously in [22]. In Sec. V, we exploit this correspondence between the WKIS system and 2D-LIA to obtain a soliton and solitary wave solutions to the 2D-LIA. Obtaining such solutions to the 2D-LIA has the benefit of providing a soliton in the natural Cartesian coordinates, while often such solitons are constructed in the curvature-torsion coordinates by use of the Hasimoto transformation between the cubic NLS and the standard LIA. As pointed out in [22], the most general purely traveling wave solution

under LIA will be a helical filament. Indeed, for the solitary waves, we find that there are two distinct wave speeds: one for the amplitude of the deflections along the filament (the wave envelope), and one that is involved with the phase of the solution. The solitary waves include two shape parameters which will alter the structure of the resulting filaments. We discuss the results and make some concluding remarks in Sec. VI.

As we progress, we relate obtained solutions to various physical scenarios of interest. For instance, the solutions of Sec. V allow us to construct the 1-soliton in the Cartesian representation under the 2D-LIA. Such solutions were observed experimentally in the 1980s. Meanwhile, the solutions of Sec. IV agree with what is observed in post reconnection events, where after vortex reconnection a sharp kink is formed and then gradually smoothed in time as Kelvin waves radiate away from the kink. Kelvin waves generated in this manner were also observed very recently in experiments in superfluid Helium, and our analytical solutions are in good qualitative agreement with the experimental observations.

II. FORMULATION OF THE PROBLEM AND CORRESPONDENCE BETWEEN THE 2D-LIA AND THE WKIS MODELS

Svistunov [2] studied vortex filament dynamics for a low-temperature superfluid in the Cartesian form, which allows one to immediately see the geometry of the line filaments. In contrast, the curvature-torsion formulation (which is what is used to map the LIA into the cubic NLS equation) requires extra effort in order to recover the Cartesian solutions. In particular, Svistunov considered the Hamiltonian formulation of the Biot-Savart dynamics (1) in Cartesian coordinates. Writing the vortex filament curve in the form $\mathbf{r}(x, t) = (x, y(x, t), z(x, t))$ and introducing a complex scalar function $w(x, t) = y(x, t) + iz(x, t)$, Svistunov obtained the Hamiltonian system

$$iw_t = \frac{\delta H[w]}{\delta w^*}, \quad (3)$$

where

$$H[w] = \frac{\Gamma}{4\pi} \int \frac{1 + \text{Re}(w_x^*(x_1, t)w_x(x_2, t))}{\sqrt{(x_1 - x_2)^2 + |w(x_1, t) - w(x_2, t)|^2}} dx_1 dx_2 \quad (4)$$

and the star denotes complex conjugation. Under the assumption that the vortex filament \mathbf{r} is of sufficient bounded variation, that is

$$|w(x_1, t) - w(x_2, t)|/|x_1 - x_2| \ll 1, \quad (5)$$

one can apply the LIA procedure to the Hamiltonian (4), obtaining the local approximation

$$\hat{H}[w] = 2\frac{\Gamma}{4\pi} \ln\left(\frac{\ell}{a}\right) \int \sqrt{1 + |w_x(x, t)|^2} dx. \quad (6)$$

If we scale time to remove the parameters multiplying the integral, we obtain the Hamiltonian formulation of the 2D-LIA,

$$iw_t = \frac{\delta \hat{H}[w]}{\delta w^*}. \quad (7)$$

The equation of motion for (7) is then

$$iw_t + \left(\frac{w_x}{\sqrt{1 + |w_x|^2}} \right)_x = 0, \quad (8)$$

and we shall refer to this as the 2D-LIA after the paper in which it was derived, [1]. This equation has been studied in a number of contexts, and once any such solution is found we directly have a solution for $\mathbf{r} = (x, \text{Re}(w), \text{Im}(w))$. Equation (8) is a scalar PDE which is of a more complicated form than the cubic NLS, hence solving this equation directly can be challenging for all but the simplest solutions. Still, some general solutions for purely rotating filaments [21] (where translation along the filament is zero) or translating waves along filaments [22] have been discussed.

The primary focus of this paper is to bring to light a relation between (8) and the integrable WKIS model studied

in [20]. Assuming w is sufficiently regular, then we can differentiate (8) with respect to the coordinate x , obtaining

$$iw_{xt} + \left(\frac{w_x}{\sqrt{1+|w_x|^2}} \right)_{xx} = 0. \quad (9)$$

Let us transform the dependent variable by $w(x, t) = \int_0^x u(\sigma, t) d\sigma$. Then, (9) takes the form

$$iu_t + \left(\frac{u}{\sqrt{1+|u|^2}} \right)_{xx} = 0, \quad (10)$$

which is exactly the WKIS model studied in [20] (in particular, this is the first equation in the WKIS hierarchy). The inverse scattering problem was discussed, and soliton solutions have been obtained. It has been shown that a generalized version of Hirota's equation with linear inhomogeneities is equivalent to a generalized continuum Heisenberg ferromagnetic spin chain equation as well as to a generalized WKIS-type equation [23]. The equivalence of generalized versions of these equations through a moving helical space curve formalism and stereographic representation was demonstrated in [24]. The scattering problem was also considered, and it was shown that an infinite number of constants of motion can exist for these systems, demonstrating the integrability of such systems. The spectral problem of the WKIS equation and certain nonlinear evolution equations related to it, the Bäcklund transformations, and the completeness relations of the eigenfunctions of the relevant generating operators were all studied in [25]. The elementary Bäcklund transformations were found and it was shown that they can be cast into a form similar to that found by Darboux for the Schrödinger spectral problem. The nonlinear superposition formulae are also explicitly written.

Though equation (10) is more complicated than the NLS or derivative-NLS equations, one can still obtain a variety of dynamics. Therefore, integrating known solutions of (10), we can immediately recover vortex filament solutions to the 2D-LIA (8). This is useful, as it spares one from solving (8) directly in those cases where a solution to (10) is already known. In this way, every solution to (10) yields a solution to (8). (Although, physically, we would want to ensure that such solutions are sufficiently well-behaved, in order to consider them candidates for vortex filament solutions.) With this in mind, we demonstrate the approach by using four classes of solutions to (10) in order to construct vortex filament solutions. In each case, we obtain solutions observed numerically and experimentally in the literature.

We should note that the condition (5) is more often approximated by $|w_x| \ll 1$, which is equivalent for most vortex structures. This condition is equivalent to saying that we expect small perturbations along what are locally line filaments. In order to get a feel for the types of solutions possible under the WKIS framework which satisfy this boundedness condition, let us assume that $w_x = O(\delta)$ for some small parameter $0 < \delta \ll 1$. Then, we may write $u = w_x = O(\delta)$. From the form of (10), it makes sense to consider a solution

$$u(x, t) = u_1\delta + u_2\delta^2 + u_3\delta^3 + O(\delta^4). \quad (11)$$

Placing (11) into (10), noting that $|u|^2 = |u_1|^2\delta^2 + O(\delta^3)$, and matching powers of the small parameter δ , we obtain

$$iu_{1t} + u_{1xx} = 0, \quad (12)$$

$$iu_{2t} + u_{2xx} = 0, \quad (13)$$

$$iu_{3t} + u_{3xx} = \frac{1}{2}(|u_1|^2 u_1)_x. \quad (14)$$

If we assume that any initial or boundary condition is at order $O(\delta)$, we may neglect u_2 since the homogeneous solution is zero. Then, we obtain $u(x, t) = u_1(x, t)\delta + u_3(x, t)\delta^3 + O(\delta^4)$, where $u_1(x, t)$ is simply a solution to the linear Schrödinger equation for a free particle and $u_3(x, t)$ is the next correction which involves solving a linear Schrödinger equation for a free particle with an external force term. Note that the force term in (14) will depend on the solution to (12) and that both (12) and (14) have the same homogeneous solution set. Therefore, one may obtain resonances in the solution of (14) which can cause the solution $u_3(x, t)$ to grow without bound, violating the requirement that $u_3 = O(1)$. Therefore, care must be taken when we are searching for solution which obey the appropriate boundedness conditions.

Once a solution $u(x, t)$ is obtained, we integrate over x in order to recover a solution to the 2D-LIA, which in turn is

used in constructing a vortex filament solution by use of $\mathbf{r}(x, t) = (x, \text{Re}[w(x, t)], \text{Im}[w(x, t)])$. Since a solution of the 2D-LIA must be of bounded variation, it suffices to consider small $|w_x| = |u|$, suggesting that small-amplitude solutions u will be the most useful to us. In what follows, we exploit the connection between the 2D-LIA and the WKIS equation to construct general stationary solutions (modeling various rotating vortex filament), similarity solutions (modeling vortex kinks), and solitons (modeling solitary pulses or waves along vortex filaments). Some of these solutions have been found in other, more involved ways under the 2D-LIA, however using the WKIS formulation we obtain these solutions rather easily and directly in Cartesian coordinates. Other solution, such as the more generalized rotating filaments, were previously obtained approximately or numerically.

III. STATIONARY STATES FOR THE WKIS EQUATION AND CORRESPONDING VORTEX FILAMENTS

We now present stationary states (solutions with time-constant modulus). While helical and planar solutions are special cases and have been shown to exist in a number of contexts, this derivation of general stationary states is new and allows us to say much about these general stationary solutions analytically rather than just numerically.

In order to more succinctly discuss the stationary states to the WKIS equation (10), let us consider the transformation

$$q = \frac{u}{\sqrt{1 + |u|^2}}, \quad (15)$$

which puts equation (10) into the form

$$i \left(\frac{q}{\sqrt{1 - |q|^2}} \right)_t + q_{xx} = 0. \quad (16)$$

It makes sense to search for a time-constant modulus solution, so we consider $q(x, t) = \Xi(x) \exp(i\tau(x, t))$. Since the phase term τ now depends on x , the stationary solutions are in general complex-valued. This results in non-planar dynamics. The transformation $q(x, t) = \Xi(x) \exp(i\tau(x, t))$ puts equation (16) into the form

$$2\Xi_x \tau_x + \Xi \tau_{xx} = 0 \quad \text{and} \quad \Xi_{xx} - \frac{\Xi \tau_t}{\sqrt{1 - \Xi^2}} - \Xi \tau_x^2 = 0. \quad (17)$$

The first equation can be integrated exactly, giving $\tau_x = C_0(t) \Xi^{-2}$, for $C_0(t) > 0$. The second equation then reads

$$\Xi_{xx} - \frac{\Xi \tau_t}{\sqrt{1 - \Xi^2}} - \frac{C_0^2(t)}{\Xi^3} = 0. \quad (18)$$

Now, Ξ is independent of time, so in order for equation (18) to be consistent we require $\tau_t = \omega$, a constant, and $C_0(t) = C_1$, another constant. With this, the phase τ is determined by Ξ like

$$\tau(x, t) = \tau_0 - \omega t + C_1^2 \int_0^x \frac{d\sigma}{\Xi(\sigma)^2}. \quad (19)$$

Meanwhile, the function Ξ is governed by the second order ODE

$$\Xi_{xx} + \frac{\omega \Xi}{\sqrt{1 - \Xi^2}} - \frac{C_1^2}{\Xi^3} = 0. \quad (20)$$

Multiplying equation (20) by $2\Xi_x$ and integrating, we obtain

$$\Xi_x^2 - 2\omega \sqrt{1 - \Xi^2} + \frac{C_1^2}{\Xi^2} = C_2, \quad (21)$$

where C_2 is another constant of integration. Equation (21) is a three-parameter ODE and can admit a variety of dynamics. Due to the form of τ , we shall seek positive solutions Ξ . Furthermore, to ensure real-valued solutions, we shall search for dynamics satisfying $0 < \Xi(x) < 1$ for all x . Transforming these solutions into vortex filament solutions

to the 2D-LIA, we should have

$$y(x, t) = \int_0^x \frac{\Xi(\sigma)}{\sqrt{1 - \Xi(\sigma)^2}} \cos \left(\tau_0 - \omega t + C_1^2 \int_0^\sigma \frac{ds}{\Xi(s)^2} \right) d\sigma, \quad (22)$$

$$z(x, t) = \int_0^x \frac{\Xi(\sigma)}{\sqrt{1 - \Xi(\sigma)^2}} \sin \left(\tau_0 - \omega t + C_1^2 \int_0^\sigma \frac{ds}{\Xi(s)^2} \right) d\sigma. \quad (23)$$

While (21) can admit a wide variety of dynamics, for sake of demonstration we shall seek a particular solution. If we desire an oscillating solution of the form $\Xi(x) = \zeta^*(1 + \delta\zeta(x) + O(\delta^2))$ for small $0 < \delta \ll 1$ and where ζ^* is an equilibrium point $0 < \zeta^* < 1$ (which makes sense in light of the $0 < \Xi(x) < 1$ condition, hence we seek a solution with small oscillations around an equilibrium point), we can then use (20) to obtain this approximate solution. The equilibrium point ζ^* satisfies the condition

$$\frac{\omega\zeta^*}{\sqrt{1 - \zeta^{*2}}} - \frac{C_1^2}{\zeta^{*3}} = 0. \quad (24)$$

The existence of such a $0 < \zeta^* < 1$ to equation (24) is equivalent to the existence of a solution $0 < \rho = \zeta^{*2} < 1$ to the polynomial equation

$$\frac{\omega^2}{C_1^4} \rho^4 + \rho - 1 = 0. \quad (25)$$

If we assume that $\rho = \zeta^{*2}$ is a solution, then we assume this polynomial has a linear factor and write the equivalent polynomial

$$\frac{\omega^2}{C_1^4} (\rho - \zeta^{*2}) \left(\rho^3 + \zeta^{*2} \rho^2 + \zeta^{*4} \rho + \zeta^{*6} + \frac{C_1^4}{\omega^2} \right) = \frac{\omega^2}{C_1^4} \rho^4 + \rho - \frac{\omega^2}{C_1^4} - \zeta^{*2}, \quad (26)$$

and these polynomials are equivalent provided

$$\frac{\omega^2}{C_1^4} + \zeta^{*2} = 1. \quad (27)$$

Thus, the polynomial equation has the root $\rho = \zeta^{*2}$ such that $\zeta^{*2} < 1$ provided

$$\zeta^* = \sqrt{1 - \frac{\omega^2}{C_1^4}}. \quad (28)$$

In turn, this implies that there exists an equilibrium solution for equation (20) provided that $C_1^2 > |\omega|$. The linear equation governing $\zeta(x)$ then becomes

$$\zeta_{xx} + \Omega^2 \zeta = 0, \quad (29)$$

where

$$\Omega^2 = \left(1 - \frac{\omega^2}{C_1^4} \right) \frac{C_1^6}{\omega^2} + C_1^2 + 3C_1^2 \left(1 - \frac{\omega^2}{C_1^4} \right)^{-2} > 0. \quad (30)$$

This then gives us $\Xi(x) = \zeta^*(1 + \delta \cos(\Omega x)) + O(\delta^2)$. Including order δ terms, we then have the solution

$$y(x, t) = \frac{C_1^2}{\omega} \sqrt{1 - \frac{\omega^2}{C_1^4}} \int_0^x \left(1 + \frac{\delta C_1^4}{\omega^2} \cos(\Omega \sigma) \right) \cos \left[\tau_0 - \omega t + C_1^2 \left(1 - \frac{\omega^2}{C_1^4} \right)^{-1} \left(\sigma - \frac{2\delta}{\Omega} \sin(\Omega \sigma) \right) \right] d\sigma, \quad (31)$$

$$z(x, t) = \frac{C_1^2}{\omega} \sqrt{1 - \frac{\omega^2}{C_1^4}} \int_0^x \left(1 + \frac{\delta C_1^4}{\omega^2} \cos(\Omega\sigma) \right) \sin \left[\tau_0 - \omega t + C_1^2 \left(1 - \frac{\omega^2}{C_1^4} \right)^{-1} \left(\sigma - \frac{2\delta}{\Omega} \sin(\Omega\sigma) \right) \right] d\sigma. \quad (32)$$

When $\delta \rightarrow 0$, we recover a helical vortex filament solution. Therefore, we can see this particular solution as a type of perturbation of the helical filament, a wavy helix. For other assumptions on the stationary solution governed by (20), other solutions would be possible. However, we have demonstrated that multiple types of stationary states (other than just planar and helix solutions) can be obtained from the WKIS equation, and these various solutions all correspond to different vortex filament structures. For small δ , we have therefore obtained a nice analytical approximation to the various generalized stationary structures studied in [21, 22], and these solution forms are perhaps a bit more succinct. We remark that the planar filament case is not exactly recovered from these solutions, since we would need $C_1 = 0$ for that case. We would have needed to set $C_1 = 0$ earlier in the calculations in order to recover that case. We shall directly consider that case, below, as it is worth working through in the WKIS setting. We will also briefly show how we can recover the standard helical case directly, without any small-amplitude approximations needed.

In Fig. 1 we give plots for various values of the parameters in (31)-(32). The solutions will take the form of deformed helices. To better view the solutions, we take a cross section in the x - y -plane, which better shows the features of the solutions than does the three-dimensional plot. We then give a three-dimensional plot of one of the representative solutions in Fig. 2. Note that the relatively simple analytical formulas allow us to recover filament curves sharing properties of the more complicated solutions in [21]. While some of the filament curves appear jagged or to have sharp kinks, the structures are actually smooth upon close inspection (as would be expected from the analytical approximations given in (31)-(32)). Further, since they are coming from (31)-(32), these solutions are of sufficient bounded variation to be considered relevant under the restrictions of the 2D-LIA.

A. The planar vortex filament reduction

There exist real-valued stationary solutions to the WKIS equation, as discussed in [28, 29]. To find such solutions, we exploit the $U(1)$ symmetry of the system and set $u(x, t) = U(x)e^{-i\omega t}$. For our purposes, we shall take $U(x)$ to be a real-valued function, as this will eventually give a planar filament.

Under the transformation of variable $U(x) = \phi(x)[1 - \phi(x)^2]^{-1/2}$ (see [29] for details) we have

$$\phi'' + \frac{\omega\phi}{\sqrt{1 - \phi^2}} = 0. \quad (33)$$

Assuming $\phi(0) = \phi_0$ and $\phi'(0) = 0$, we obtain

$$\phi'^2 = 2\omega \left(\sqrt{1 - \phi^2} - \sqrt{1 - \phi_0^2} \right), \quad (34)$$

which gives the implicit representation

$$\sqrt{2\omega}x = \int_{\phi_0}^{\phi(x)} \frac{d\nu}{\sqrt{\sqrt{1 - \nu^2} - \sqrt{1 - \phi_0^2}}}. \quad (35)$$

The corresponding planar solution for the 2D-LIA is then immediately found to be

$$w(x, t) = e^{-i\omega t} \int_0^x U(\sigma) d\sigma = e^{-i\omega t} \int_0^x \frac{\phi(\sigma) d\sigma}{\sqrt{1 - \phi(\sigma)^2}} = -e^{-i\omega t} \int_0^x \frac{\phi''(\sigma)}{\omega} d\sigma = -\frac{1}{\omega} e^{-i\omega t} \phi'(x). \quad (36)$$

Hence, by solving the differential equation (34), we immediately obtain the stationary solution desired. The planar solution can then be recovered by $\mathbf{r}(x, t) = (x, -\omega^{-1}\phi'(x)\cos(\omega t), \omega^{-1}\phi'(x)\sin(\omega t))$. We plot a representative planar vortex filament solution in Fig. 3.

Planar vortex filaments have previously been studied in other settings, including for the standard LIA (2) and other related models [4, 30–34]. Purely rotating filaments were studied for the 2D-LIA in [21], and these hold the planar filaments as special cases. Regarding the 2D-LIA, such planar filament solutions were constructed using a direct approach. However, as we have seen here, one may also obtain such solutions through the correspondence with the WKIS model. Naturally, the solutions we obtain here agree with those obtained by other approaches in the literature.

In the warmer temperature regime, mutual friction and normal fluid effects will matter, and such effects are taken

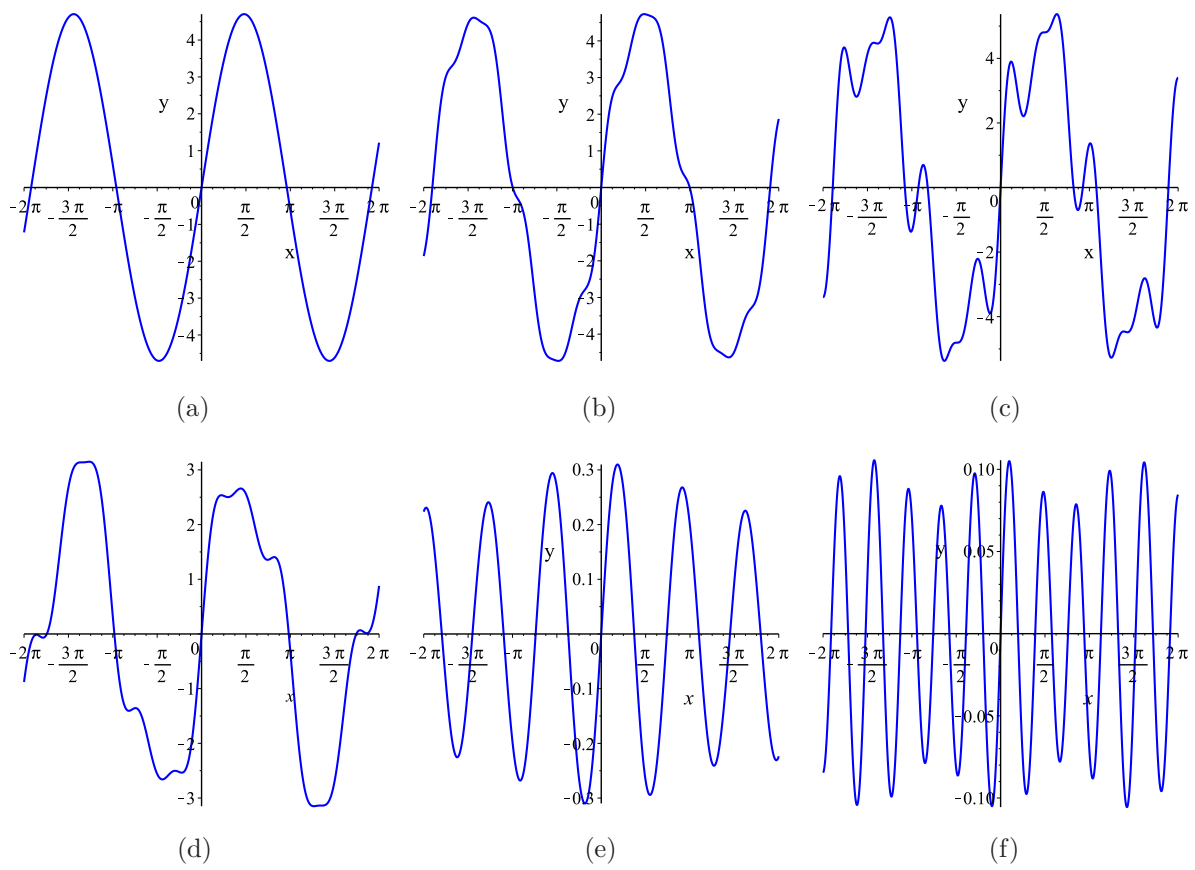


FIG. 1: Plots of various generalized stationary solutions given by (31)-(32). Here we plot cross sections of the vortex filament solutions in the $x - y$ -plane. We take $\tau_0 = 0$, and vary the small parameter δ and the shape parameter ω , with values (a) $\delta = 0, \omega = 0.2$, (b) $\delta = 0.03, \omega = 0.2$, (c) $\delta = 0.1, \omega = 0.2$, (d) $\delta = 0.1, \omega = 0.3$, (e) $\delta = 0.1, \omega = 0.8$, (f) $\delta = 0.1, \omega = 0.9$. We fix $C_1 = 1$, as only the relative values of C_1 and ω will matter. We need $C_1 > \sqrt{|\omega|} > 0$, which is why $0 < \omega < 1$ in the various plots provided. The solutions are plotted for $t = 0$, and the solutions maintain their form and rotate in time, so this choice is sufficiently general in order to view the filament structure. Corresponding Cartesian three-dimensional representations of the vortex filament curves are given in Fig. 2. Note that panel (a) corresponds to a regular helical filament in the limit $\delta = 0$, while the others correspond to generalized, less regular forms.

into account in the Schwarz model [35]. It was shown in [36] that purely planar filaments should be expected in the classical LIA, or in the zero-temperature limit for the quantum model, while they will not exist in the presence of mutual friction and normal fluid flow due to the induced torsion due to these small terms. The result will be a twisted planar filament. In other words, if we begin with a planar filament as the initial data at time $t = 0$, the time evolution of this initial condition will result in a twisted form of this initial data which no longer is confined to a plane.

B. The helical filament reduction

Let us show that planar wave solutions of the WKIS model yield helical vortex filaments under the 2D-LIA. Assume $u(x, t) = a \exp(i \{kx - \Omega t + j\})$, where a, k, Ω, j are constants. Placing this into (10), we obtain the dispersion relation $\Omega = k^2 / \sqrt{1 + a^2}$, which is exactly the dispersion relation found in the literature for the direct 2D-LIA problem. A solution w to the 2D-LIA (8) then takes the form

$$w(x, t) = -i \frac{a}{k} \exp \left(i \left\{ kx - \frac{k^2}{\sqrt{1 + a^2}} t + j \right\} \right) = A \exp \left(i \left\{ kx - \frac{k^2}{\sqrt{1 + A^2 k^2}} t + \hat{j} \right\} \right). \quad (37)$$

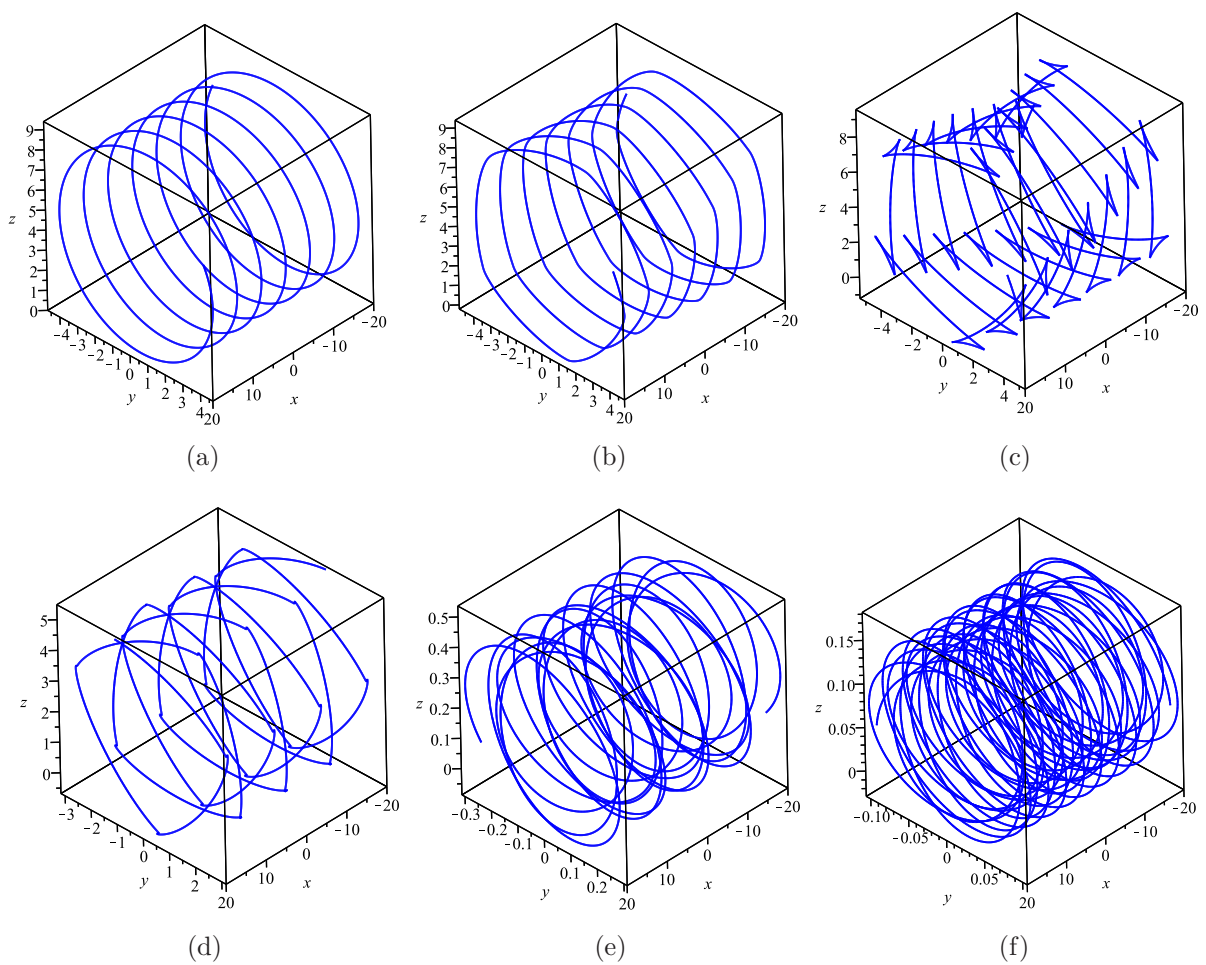


FIG. 2: Three-dimensional Cartesian representations of the vortex filament solutions for which we considered cross sections in Fig. 1. We take $\tau_0 = 0$, and vary the small parameter δ and the shape parameter ω , with parameters fixed as (a) $\delta = 0, \omega = 0.2$, (b) $\delta = 0.03, \omega = 0.2$, (c) $\delta = 0.1, \omega = 0.2$, (d) $\delta = 0.1, \omega = 0.3$, (e) $\delta = 0.1, \omega = 0.8$, (f) $\delta = 0.1, \omega = 0.9$. We fix $C_1 = 1$, as only the relative values of C_1 and ω will matter. We need $C_1 > \sqrt{|\omega|} > 0$, which is why $0 < \omega < 1$ in the various plots provided. The solutions are plotted for $t = 0$, and the solutions maintain their form and rotate in time, so this choice is sufficiently general in order to view the filament structure. Note that panel (a) corresponds to a regular helical filament in the limit $\delta = 0$, while the others correspond to generalized, less regular forms. While some of the filament curves may appear to be jagged, if one zooms in close enough, all structures are actually smooth.

Pick parameters $A = a/k$ and $\hat{j} = j - \frac{\pi}{2}$. Then, the helical filament has the structure

$$\mathbf{r}(x, t) = \left(x, A \cos \left(kx - \frac{k^2}{\sqrt{1 + A^2 k^2}} t + \hat{j} \right), A \sin \left(kx - \frac{k^2}{\sqrt{1 + A^2 k^2}} t + \hat{j} \right) \right). \quad (38)$$

These are exactly the solutions one obtains directly [37], which should not be surprising. In the very low temperature limit, the helical filaments are eternal. However, in the warmer superfluid regime (say, temperatures near 1K), mutual friction effects and the normal fluid flow can amplify Kelvin waves along line filaments (realized mathematically as helical filaments) due to the Donnelly-Glaberson instability [38–40]. Therefore, the helical filaments can decay or amplify when mutual friction and normal fluid velocity are included, such as in the Schwarz model [35]. The nonlinear dynamics of such Kelvin waves under the Schwarz model were recently studied in [41], where it was shown that the rate of amplification or decay of Kelvin waves along these quantum vortex filaments will depend strongly on the mutual friction parameter, with the rate becoming larger as the superfluid warms. Helical filaments in both classical and quantum fluids continue to be an active area of research interest [42–45].

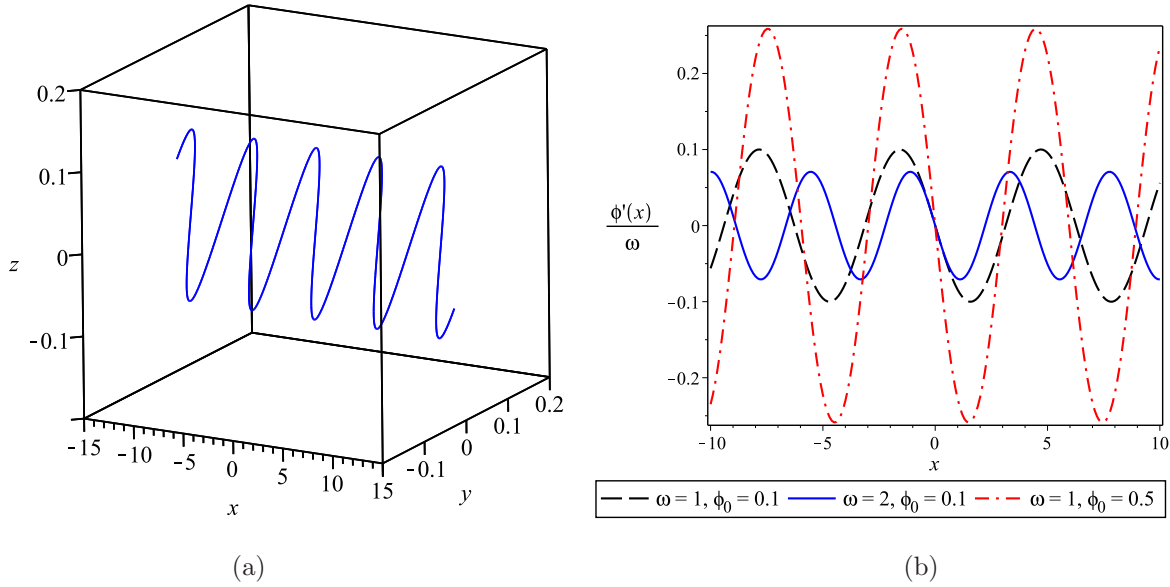


FIG. 3: (a) Plot of a planar filament solution $\mathbf{r}(x, t) = (x, -\omega^{-1}\phi'(x)\cos(\omega t), \omega^{-1}\phi'(x)\sin(\omega t))$ in space when $\omega = 1$ and $\phi_0 = 0.1$. A value of $t = 2$ is used for the time variable, but motion of the filament is that of a pure rotation around the x -axis with period $\frac{2\pi}{\omega}$. The entire spatial structure of the filament maintains its form under this periodic motion. (b) Plots of the function $\omega^{-1}\phi'(x)$ used to generate the planar vortex filaments, for various values of the spectral parameter ω and initial condition $\phi(0) = \phi_0$.

IV. SIMILARITY SOLUTIONS AND VORTEX KINKS

Self-similar solutions have been studied in different but related models for vortex filament dynamics. Therefore, we now show that self-similar solutions are possible under the 2D-LIA by means of the WKIS model. Note that the author has not seen a treatment of self-similar solutions for any member of the WKIS hierarchy, and hence such solutions may be of use for other applications relating to the WKIS hierarchy.

For equation (10), we assume $u(x, t) = f(\chi)$ where $\chi = x/\sqrt{2t}$, which gives

$$-i\chi \frac{df}{d\chi} + \frac{d^2}{d\chi^2} \left(\frac{f}{\sqrt{1+|f|^2}} \right) = 0. \quad (39)$$

One then may recover the self-similar solution to the 2D-LIA via

$$w(x, t) = \int_0^x u(q, t) dq = \int_0^x f\left(\frac{q}{\sqrt{2t}}\right) d\chi dq. \quad (40)$$

There is no exact solution to equation (39) in general, owing to the nonlinearity. However, if we assume a small amplitude solution $f(\chi) = \beta F(\chi)$ for small parameter β , corresponding to small deformations of the vortex line, then we arrive at the linearized equation

$$-i\chi \frac{dF}{d\chi} + \frac{d^2 F}{d\chi^2} = O(\beta^2). \quad (41)$$

This gives a solution $f(\chi) = \beta \int_0^\chi \exp\left(\frac{i}{2}\sigma^2\right) d\sigma + O(\beta^3)$. Recovering

$$w(x, t) = \beta \int_0^x \int_0^{q/\sqrt{2t}} \exp\left(\frac{i}{2}\sigma^2\right) d\sigma dq + O(\beta^3), \quad (42)$$

we obtain the vector representation for the vortex filament as

$$\mathbf{r}(x, t) = \left(x, \beta \int_0^x \int_0^{q/\sqrt{2t}} \cos\left(\frac{1}{2}\sigma^2\right) d\sigma dq + O(\beta^3), \beta \int_0^x \int_0^{q/\sqrt{2t}} \sin\left(\frac{1}{2}\sigma^2\right) d\sigma dq + O(\beta^3) \right). \quad (43)$$

A. Boundedness of similarity solutions in variation

One may show that there exist positive constants C_1 and C_2 such that the solution (43) must remain bounded like $|\mathbf{r}(x, t)| < C_1|x| + C_2$ for all $t \geq 0$. Similar to the arguments presented in [22] for the boundedness for solutions to the 2D-LIA, for small enough C_1 the solution (43) will be of sufficient bounded variation to justify the application of the 2D-LIA. Therefore, while there can be a sharp kink at the origin, for any positive $t > 0$, the filament curves will be of bounded variation.

More formally, note that

$$w_x = \beta \int_0^{x/\sqrt{2t}} \exp\left(\frac{i}{2}\sigma^2\right) d\sigma, \quad (44)$$

hence

$$\begin{aligned} |w_x| &= |\beta| \left| \int_0^{x/\sqrt{2t}} \left\{ \cos\left(\frac{1}{2}\sigma^2\right) + i \sin\left(\frac{1}{2}\sigma^2\right) \right\} d\sigma \right| \\ &= \sqrt{\pi}|\beta| \left| \text{FresnelC}\left(\frac{x}{\sqrt{2\pi t}}\right) + i \text{FresnelS}\left(\frac{x}{\sqrt{2\pi t}}\right) \right| \\ &= \sqrt{\pi}|\beta| \sqrt{\text{FresnelC}\left(\frac{x}{\sqrt{2\pi t}}\right)^2 + \text{FresnelS}\left(\frac{x}{\sqrt{2\pi t}}\right)^2} \\ &< 1.69|\beta|. \end{aligned} \quad (45)$$

Therefore,

$$\lim_{x_2 \rightarrow x} \frac{|w(x, t) - w(x_2, t)|}{|x - x_2|} = |w_x| < 1.69|\beta|, \quad (46)$$

so we need $|\beta| \ll 1$ in order for the vortex filament curve to be of sufficient bounded variation. Then, the assumption that $f(\chi) = \beta F(\chi)$ for $|\beta| \ll 1$ made above is completely reasonable. From the form of (43) we then have that

$$|\mathbf{r}(x, t)| < |x| + 1.69|\beta||x| + C_2 < C_1|x| + C_2, \quad (47)$$

if we pick $C_1 > 1 + 1.69|\beta|$. Therefore, the self similar solution (43) does indeed obey a bound of the form $|\mathbf{r}(x, t)| < C_1|x| + C_2$ for all $t \geq 0$.

The above derivation shows that solutions are of bounded variation in the weak sense, that is $|w_x| \ll 1$. In order to show that these solutions are of bounded variation in the strong sense of (5), observe that

$$\begin{aligned} \left| \frac{w(x_1, t) - w(x_2, t)}{x_1 - x_2} \right| &= \frac{\left| \int_{x_2}^{x_1} f\left(\frac{q}{\sqrt{2t}}\right) dq \right|}{|x_1 - x_2|} \\ &= \frac{\left| \int_{x_2}^{x_1} \int_0^{q/\sqrt{2t}} \left\{ \beta \exp\left(\frac{i}{2}\sigma^2\right) d\sigma + O(\beta^3) \right\} dq \right|}{|x_1 - x_2|} \\ &\leq \frac{\left| \int_{x_2}^{x_1} |1.69\beta + O(\beta^3)| dq \right|}{|x_1 - x_2|} \\ &\leq \frac{|1.69\beta||x_1 - x_2|}{|x_1 - x_2|} + O(\beta^3) \\ &= 1.69|\beta| + O(\beta^3). \end{aligned} \quad (48)$$

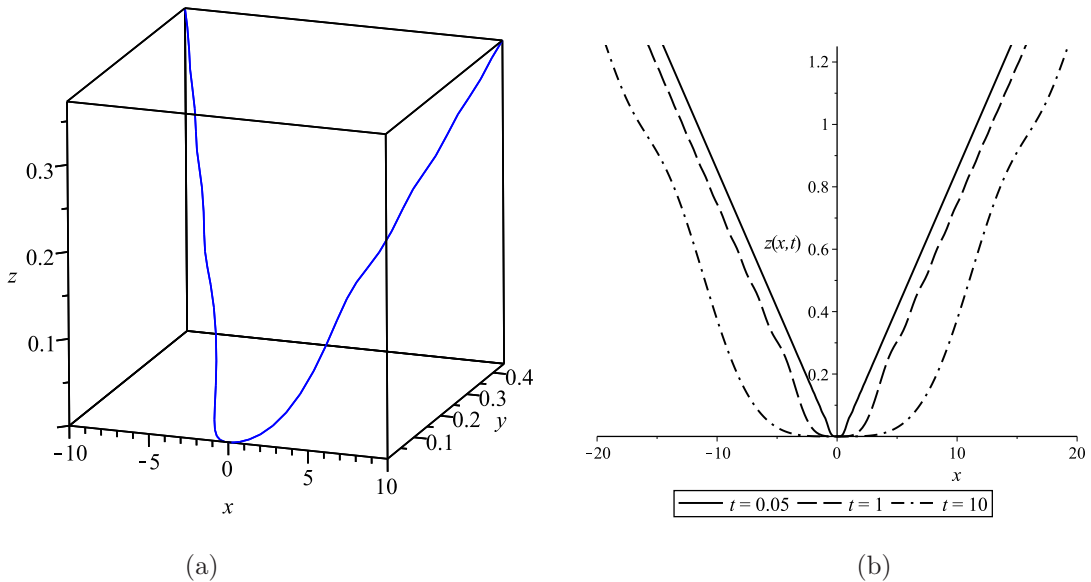


FIG. 4: Plot of self-similar wave structures along a vortex filament. (a) We use the approximate solution (43) and take the amplitude of the waves to be of size $\beta = 0.05$. Time is taken to be $t = 1$. As time increases, the waves broaden and propagate away from the origin. This gives the appearance of a wavy V-shaped curve that smooths over time. (b) We obtain numerical solutions to the ODE governing a self-similar solution, and upon recovering the Cartesian representation, we plot the cross section of the exact self-similar solution in the x - z plane. In this case, the amplitude parameter corresponds to $\beta = 0.1$. The plots clearly show the time evolution of the vortex filament: For very small values of time, there is a very sharp kink at the origin, and this kink smooths as time increases.

As such, we have shown that the approximation to the similarity solution will satisfy

$$\left| \frac{w(x_1, t) - w(x_2, t)}{x_1 - x_2} \right| < 1 \quad (49)$$

for small $|\beta| \ll 1$, hence it satisfies the strong form of the bounded variation restriction given in (5).

B. Behavior of similarity solutions

We provide a plot of self-similar waves along a vortex filament in Fig. 4. In Fig. 4(a) we plot the analytical approximation corresponding to (43). Meanwhile, in Fig. 4(b) we plot the numerical solution for the exact problem (39). There is strong agreement between analytical approximations and the numerical solutions when the amplitude of the waves along the V-shaped filaments is small. This small amplitude regime is consistent with the requirement that the vortex filament curves be of bounded variation.

These kinds of solutions have been observed in the literature for vortex filaments in various physical scenarios through experiments, numerical simulations, and theoretical studies. Theoretical and analytical studies of self-similar vortex filament dynamics in superfluids demonstrate that a wide variety of behaviors are possible [46–48], including the behaviors displayed here in the very low temperature limit. More mathematical papers have considered the existence of self-similar structures for the LIA and related problems (such as the relevant cubic NLS dynamics), see [49–52].

Interestingly, the solutions appear quite similar to post-reconnection events. In such events, two vortex filaments swap tails resulting in two new V-shaped filaments. This process is necessarily discontinuous at the time of the filament-filament intersection. If the reconnection event occurs at time $t = 0$, then we can view $t > 0$ dynamics as the post reconnection time evolution of the newly formed filament. At the moment of reconnection, the filament would take the form of a V with a sharp kink at the origin (the curve would fail to have a well-defined derivative at $x = 0$, which we take to be the location of the kink). Then, as time increases, the sharp kink would smooth, resulting in a smooth vortex filament. This is exactly what we see for $t > 0$, and hence the self-similar solutions shown here are reasonable approximations to post reconnection events. At very small values of time, there is very large curvature at the origin, and this curvature is transported along the vortex filament curve resulting in a smoothing of the kink, as best seen in Figure 4(b).

This type of reconnection scenario was theoretically considered in [53]. However, rather recently there were experimental results [54] which showed that Kelvin waves radiate away from the kinks formed after reconnection events. That is to say, the V-shaped filaments have Kelvin waves which propagate outward from the kink along the two line segments that make up the vortex filament. These experimental results are in complete agreement with the self-similar vortex filament dynamics we obtain above. A sharp vortex kink exists at time $t = 0$, and this kink gradually smooths as Kelvin waves radiate away from it. This is precisely the time evolution observed in Fig. 4. Hence, the self-similar solutions we obtain are in nice qualitative agreement with the dynamics observed experimentally in [54].

In addition to the interesting vortex filament dynamics we discuss above, the results here are also interesting as they are the first attempt at a study of the self-similar dynamics arising from the WKIS equations. Indeed, the author is not aware of any other studies regarding self-similarity within the framework of the WKIS hierarchy. However, due to the relations between some members of this integrable hierarchy and other, more well-known integrable systems, the existence of self-similarity in these equations should be anticipated. The form of self-similarity is different from that one expects from equations such as the diffusion equation or the cubic NLS equation: Often, there is a coefficient of $t^{-1/2}$ or $t^{1/2}$ multiplying the unknown function, yet the WKIS equations only involve the time variable within the similarity variable, preventing any blow-up or singularity provided that the similarity function remains bounded.

V. SOLITARY WAVES ALONG VORTEX FILAMENTS UNDER THE 2D-LIA

The author is not aware of any soliton solutions to the 2D-LIA, likely owing to the fact that the governing PDE is more complicated than the cubic NLS (which of often what is used to construct soliton solutions on vortex filaments). Usually, one obtains the soliton solution of the NLS equation, which from the Hasimoto map can be put into correspondence with the curvature and torsion of an LIA solution. Then, one integrates the Frenet-Serre formulas in order to recover the tangent, normal, and bi-normal vectors. Finally, one integrates along the tangent vector to obtain a particular vortex filament curve. We bypass this procedure, since we can directly obtain a vortex filament curve from the 2D-LIA once a WKIS solution is known.

Since the soliton solutions to the WKIS model are reasonably well studied, we can use these in order to construct solution solution to the 2D-LIA. Under the framework laid out for the one-soliton solution of (10) in [20], we can obtain immediately the one-soliton for the 2D-LIA using $w(x, t) = \int_0^x u(\sigma, t) d\sigma$. In terms of the coordinates y and z , we have

$$y(x, t) = \frac{-|\xi|\eta}{\xi^2 + \eta^2} \int_0^x \frac{\cosh(A(\sigma, t)) \cos(B(\sigma, t))}{\cosh^2(A(\sigma, t)) - \frac{2\eta^2}{\xi^2 + \eta^2}} d\sigma + \frac{\xi}{|\xi|} \frac{\eta^2}{\xi^2 + \eta^2} \int_0^x \frac{\sinh(A(\sigma, t)) \sin(B(\sigma, t))}{\cosh^2(A(\sigma, t)) - \frac{2\eta^2}{\xi^2 + \eta^2}} d\sigma, \quad (50)$$

$$z(x, t) = \frac{|\xi|\eta}{\xi^2 + \eta^2} \int_0^x \frac{\cosh(A(\sigma, t)) \sin(B(\sigma, t))}{\cosh^2(A(\sigma, t)) - \frac{2\eta^2}{\xi^2 + \eta^2}} d\sigma + \frac{\xi}{|\xi|} \frac{\eta^2}{\xi^2 + \eta^2} \int_0^x \frac{\sinh(A(\sigma, t)) \cos(B(\sigma, t))}{\cosh^2(A(\sigma, t)) - \frac{2\eta^2}{\xi^2 + \eta^2}} d\sigma, \quad (51)$$

where $A(x, t) = 2\eta(1 + \epsilon)(x + 4\xi t)$, $B(x, t) = 2\xi x + 4(\xi^2 - \eta^2)t + 2\xi\epsilon(x + 4\xi t)$ are distinct wave-like variables, ξ and η are parameters modifying the shape of the WKIS soliton, and $\epsilon(q)$ is a function satisfying the implicit algebraic relation

$$\epsilon(q) = \frac{\eta}{\xi^2 + \eta^2} (\tanh(2\eta[q + \epsilon(q)]) - 1). \quad (52)$$

As discussed in [22], the only purely traveling wave solutions to the 2D-LIA are those which take the form of a helix. In order to obtain more complicated solitary waves, we have needed to introduce two competing wave variables, $x + 4\xi t$, which enters into both $A(x, t)$ and $B(x, t)$, and $x + 2\xi^{-1}(\xi^2 - \eta^2)t$, which enters into only $B(x, t)$.

The greatest complication here is obtaining the implicitly defined function ϵ give through (52). In Fig. 5 we give numerical plots of ϵ as a function of q for various values of η and ξ . The curve ϵ is a well-defined function of q provided that ξ is not too small. In the limit where $\xi \rightarrow 0$, the curve ϵ becomes multi-valued in q in a region near the origin. This happens when the change in ϵ with q becomes infinite at a point. If we were to reverse the formal relation between ϵ and q , this would be equivalent to the point at which there is zero change in q with a change in ϵ . There should be some critical value $\xi = \xi_c > 0$ for which this occurs. For $|\xi| < \xi_c$, the relation will be multi-valued. For $|\xi| > \xi_c$, there is a well-defined function $\epsilon = \epsilon(q)$ from the relation (52).

In order to obtain the critical value ξ_c , let us write the expression (52) so that it describes a function $q(\epsilon)$. Differ-

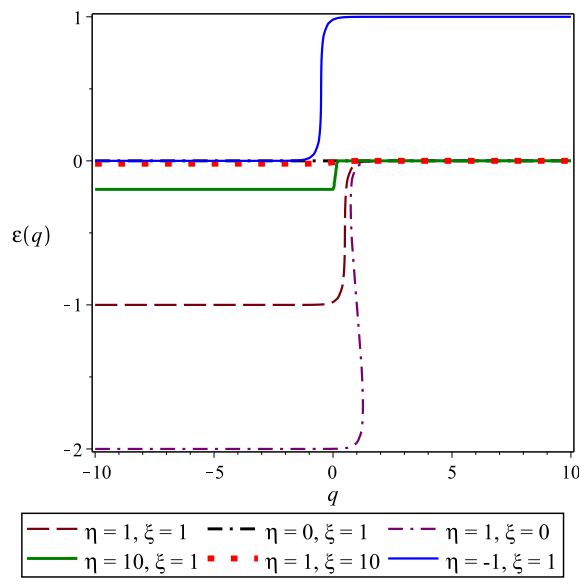


FIG. 5: Plot $\epsilon(q)$ from the implicit relation (52). The solution will be sensitive to the sign of η but not ξ . The curve ϵ is a well-defined function of q provided that ξ is not too small. In the limit where $\xi \rightarrow 0$, the curve ϵ becomes multi-valued in q in a region near the origin.

entiation of (52) in terms of ϵ , we find

$$1 = \frac{2\eta^2}{\xi^2 + \eta^2} \text{sech}^2(2\eta(q + \epsilon)) \left\{ \frac{dq}{d\epsilon} + 1 \right\}. \quad (53)$$

At the critical value ξ_c , we must have $\frac{dq}{d\epsilon} = 0$ (which is equivalent to $\left| \frac{dq}{d\epsilon} \right| \rightarrow \infty$). In particular, there will be two such ϵ values for $|\xi| < \xi_c$, one value for $|\xi| = \xi_c$, and no such values for $|\xi| > \xi_c$.

Taking $\frac{dq}{d\epsilon} = 0$ in (53), we have

$$1 = \frac{2\eta^2}{\xi^2 + \eta^2} \text{sech}^2(2\eta(q + \epsilon)). \quad (54)$$

Combining (52) and (54), we obtain

$$1 + 4\eta\epsilon^* + 2(\xi^2 + \eta^2)(\epsilon^*)^2 = 0, \quad (55)$$

and this gives the roots

$$\epsilon^* = -\frac{2\eta \pm \sqrt{2(\eta^2 - \xi^2)}}{2(\eta^2 + \xi^2)}. \quad (56)$$

When $|\xi| < |\eta|$ we have two roots, while when $|\xi| > |\eta|$ we have no roots. When $|\xi| = |\eta|$ we have exactly one root, and by our discussion above, we obtain the critical value $\xi_c = |\eta|$.

From this we see that (52) can be interpreted as the intersection of a straight line with a stretched and horizontally shifted tanh function of ϵ , and equation (54) corresponds to the condition of tangent intersection. When there are two roots to (55), there can be two such intersections, highlighting the multi-valued property of the relation when $|\xi| < \xi_c$.

Assuming then that $|\xi| > \xi_c$, note from (52) that we have the limits

$$\lim_{q \rightarrow \pm\infty} \epsilon(q) = \frac{\eta}{\xi^2 + \eta^2} (\pm \text{sgn}(\eta) - 1). \quad (57)$$

We have two possibilities. If $\eta > 0$, then $\epsilon \rightarrow 0$ as $q \rightarrow \infty$, while $\epsilon \rightarrow -\frac{2\eta}{\xi^2 + \eta^2} < 0$ as $q \rightarrow -\infty$. Meanwhile, if $\eta < 0$, then $\epsilon \rightarrow -\frac{2\eta}{\xi^2 + \eta^2} = \frac{2|\eta|}{\xi^2 + \eta^2} > 0$ as $q \rightarrow \infty$, while $\epsilon \rightarrow 0$ as $q \rightarrow -\infty$. This suggests that the solutions $\epsilon(q)$ themselves

should take a form much like tanh profiles, and this is supported by the numerical solutions in Fig. 5. From those numerical plots, we see that the curves are not exactly symmetric about the origin. Rather, we see that the midpoint (between the maximal and minimal value) occurs for

$$\epsilon_{\text{mid}} = -\frac{\eta}{\xi^2 + \eta^2}, \quad (58)$$

and this actually gives, from (52), that

$$-\frac{\eta}{\xi^2 + \eta^2} = \frac{\eta}{\xi^2 + \eta^2} \left(\tanh \left(2\eta \left[q_{\text{mid}} - \frac{\eta}{\xi^2 + \eta^2} \right] \right) - 1 \right). \quad (59)$$

Solving this, we must have

$$q_{\text{mid}} - \frac{\eta}{\xi^2 + \eta^2} = 0, \quad (60)$$

and so

$$q_{\text{mid}} = \frac{\eta}{\xi^2 + \eta^2}. \quad (61)$$

Therefore, we can approximate the solution for $\epsilon(q)$ by

$$\epsilon(q) \approx \frac{\eta}{\xi^2 + \eta^2} \left\{ \tanh \left(2\eta \left[q - \frac{\eta}{\xi^2 + \eta^2} \right] \right) - 1 \right\}. \quad (62)$$

This approximation is reasonable for $|\xi| > \xi_c$. In this regime, we may therefore approximate the functions of wave variables like

$$A(x, t) \approx 2\eta x + 8\eta \xi t - \frac{2\eta^2}{\xi^2 + \eta^2} \left\{ 1 - \tanh \left(2\eta \left[x + 4\xi t - \frac{\eta}{\xi^2 + \eta^2} \right] \right) \right\}, \quad (63)$$

$$B(x, t) \approx 2\xi x + 4(\xi^2 - \eta^2)t - \frac{2\xi\eta}{\xi^2 + \eta^2} \left\{ 1 - \tanh \left(2\eta \left[x + 4\xi t - \frac{\eta}{\xi^2 + \eta^2} \right] \right) \right\}. \quad (64)$$

From this analysis, we see that the function $\epsilon(q) = O(1)$ in q and hence can be treated as a constant in most instances. Doing so, we obtain from (50)-(51) the approximations

$$\begin{aligned} y(x, t) \approx & -\frac{|\xi|\eta}{\xi^2 + \eta^2} \int_{x_0}^x \frac{\cosh(2\eta\sigma + 8\xi\eta t) \cos(2\xi x + 4(\xi^2 - \eta^2)t - x_1)}{\cosh^2(2\eta\sigma + 8\xi\eta t) - \frac{2\eta^2}{\xi^2 + \eta^2}} d\sigma \\ & + \text{sgn}(\xi) \frac{\eta^2}{\xi^2 + \eta^2} \int_{x_0}^x \frac{\sinh(2\eta\sigma + 8\xi\eta t) \sin(2\xi x + 4(\xi^2 - \eta^2)t - x_1)}{\cosh^2(2\eta\sigma + 8\xi\eta t) - \frac{2\eta^2}{\xi^2 + \eta^2}} d\sigma, \end{aligned} \quad (65)$$

$$\begin{aligned} z(x, t) \approx & \frac{|\xi|\eta}{\xi^2 + \eta^2} \int_{x_0}^x \frac{\cosh(2\eta\sigma + 8\xi\eta t) \sin(2\xi x + 4(\xi^2 - \eta^2)t - x_1)}{\cosh^2(2\eta\sigma + 8\xi\eta t) - \frac{2\eta^2}{\xi^2 + \eta^2}} d\sigma \\ & + \text{sgn}(\xi) \frac{\eta^2}{\xi^2 + \eta^2} \int_{x_0}^x \frac{\sinh(2\eta\sigma + 8\xi\eta t) \cos(2\xi x + 4(\xi^2 - \eta^2)t - x_1)}{\cosh^2(2\eta\sigma + 8\xi\eta t) - \frac{2\eta^2}{\xi^2 + \eta^2}} d\sigma, \end{aligned} \quad (66)$$

where we introduce constants x_0 and x_1 to approximate the effect of treating $\epsilon(q)$ as a constant in the phase and amplitude parts of the solutions.

We may now consider some special cases. First, in the limit where $\xi^2 \gg \eta^2$ (in which the phase of the soliton is rapidly varying compared with the amplitude) we have

$$y(x, t) \approx -\frac{\eta}{\xi} \int_0^x \text{sech}(2\eta[\sigma + 4\xi t]) \cos(2\xi\sigma + 4\xi^2 t) d\sigma, \quad (67)$$

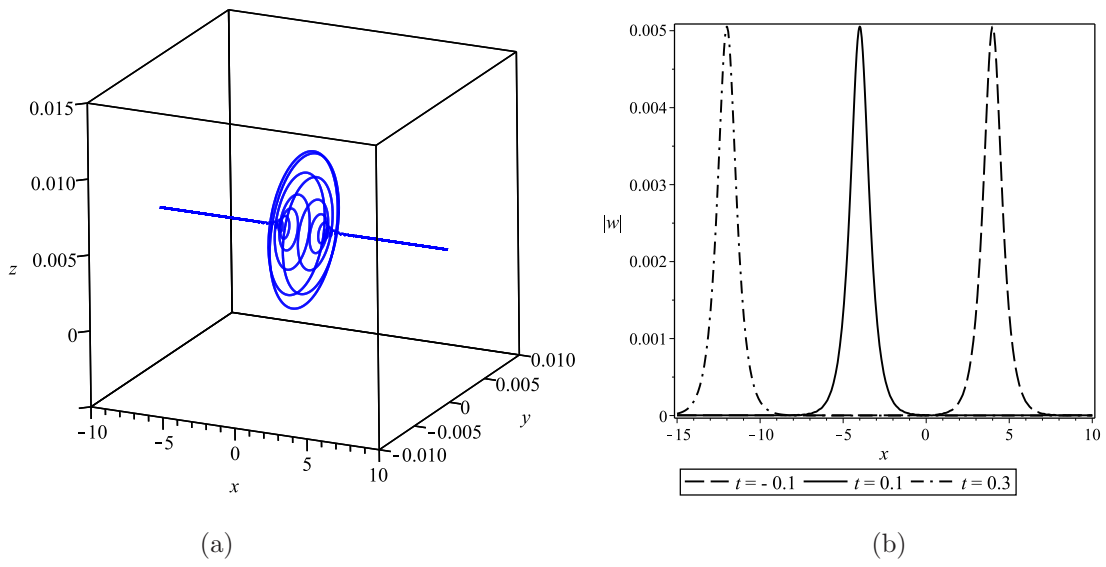


FIG. 6: Plot of a one-soliton solution (67)-(68) in space when $\xi = 10$ and $\eta = 1$, satisfying $\xi^2 \gg \eta^2$. The twisting of the vortex filament line is due to the torsion effects governing the dynamics. Maximal curvature occurs at the envelope peak. In (a) we plot the vortex filament in Cartesian coordinates at time $t = 0$. A value of $t = 0$ is used for the plot, but the wave envelope maintains its form and propagates toward the left along the x -axis as time increases. In (b) we plot the modulus $|w(x, t)| = \sqrt{y(x, t)^2 + z(x, t)^2}$ for various values of time, so that we may better view the wave envelope.

$$z(x, t) \approx \frac{\eta}{\xi} \int_0^x \text{sech}(2\eta[\sigma + 4\xi t]) \sin(2\xi\sigma + 4\xi^2 t) d\sigma. \quad (68)$$

Such a soliton is qualitatively similar to the NLS one-soliton. In Fig. 6 we plot a representative soliton solution. We see that the soliton consists of an envelope which propagates toward the negative x direction. Along this envelope, the filament twists due to torsion effects. The curvature maximum occurs at the center of the envelope. Away from the center of the envelope, the filament behaves like a line filament. This solution may thus be considered as a solitary wave or topological defect which moves along a line filament. Once this solitary wave passes, the filament locally returns to its prior line filament configuration. Such solutions as those displayed here are consistent with both analytical [6, 16, 17] and experimental [12–14] results in the literature, as were discussed in Section 1. These particular specific solutions will exhibit rotation about the x -axis (due to the sine and cosine terms), while the wave packet itself will translate along the x -axis (due to the sech terms).

In the limit where $\xi \rightarrow 0$, $y = z = 0$, and we recover a line filament. Similarly, when $\eta \rightarrow 0$, we have $y = z = 0$, and hence the solutions collapse to a line filament.

In the case where $\xi = \eta$, the solutions (65)-(66) reduce to

$$y(x, t) \approx -\frac{\text{sgn}(\eta)}{2} \int_{x_0}^x \frac{\cosh(2\eta\sigma + 8\eta^2 t) \cos(2\eta x - x_1)}{\cosh^2(2\eta\sigma + 8\eta^2 t) - 1} d\sigma + \frac{\text{sgn}(\eta)}{2} \int_{x_0}^x \frac{\sinh(2\eta\sigma + 8\eta^2 t) \sin(2\eta x - x_1)}{\cosh^2(2\eta\sigma + 8\eta^2 t) - 1} d\sigma, \quad (69)$$

$$z(x, t) \approx \frac{\text{sgn}(\eta)}{2} \int_{x_0}^x \frac{\cosh(2\eta\sigma + 8\eta^2 t) \sin(2\eta x - x_1)}{\cosh^2(2\eta\sigma + 8\eta^2 t) - 1} d\sigma + \frac{\text{sgn}(\eta)}{2} \int_{x_0}^x \frac{\sinh(2\eta\sigma + 8\eta^2 t) \cos(2\eta x - x_1)}{\cosh^2(2\eta\sigma + 8\eta^2 t) - 1} d\sigma. \quad (70)$$

Note that the rotational part of the solutions (the sin and cos functions) are now independent of time. Therefore, the solutions will not tend to rotate around the reference axis. The time dependence is now strictly in the terms governing the wave envelope, and the solutions will maintain their form while translating along the reference axis. Note that these solutions develop a singularity when $2\eta\sigma + 8\eta^2 t = 1$, which would give the solutions an appearance

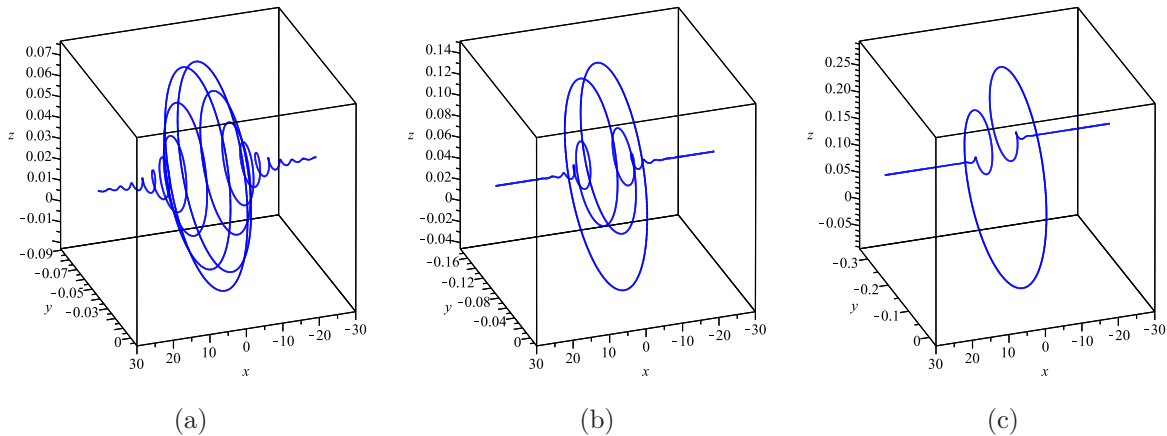


FIG. 7: Three-dimensional Cartesian representations of the solitary waves along vortex filaments. Parameter values are $x_0 = 0$, $x_1 = 1$, $\xi = 1$, and we plot the solutions for various $\eta > 0$: (a) $\eta = 0.1$, (b) $\eta = 0.2$, (c) $\eta = 0.4$. As we take $\eta \rightarrow \xi$ from below, the oscillations in the filament curve die off.

like a breather at certain locations. In order to avoid such situations, one should consider a restriction

$$0 < \frac{2\eta^2}{\xi^2 + \eta^2} < 1, \quad (71)$$

which is equivalent to $0 < |\eta| < |\xi|$. So, we can view the $\xi = \eta$ case at the upper limit to this restriction, and hence the irrotational solutions (69)-(70) can be considered as the least regular physical solutions possible under this reduction. What this means is that, for $0 < |\eta| < |\xi|$, there will always be a non-trivial rotational component to the solitary waves in time. Therefore, solitary wave solutions will tend to both translate along the reference axis while also rotating along the reference axis. This is a property they share with other solutions, such as the helical filaments. In contrast, the rate of rotation and translation will differ, due to the appearance of two different wavespeeds in the solutions. This is in contrast to the helix, which has one wavespeed (as discussed in [22]).

In Fig. 7 we provide solitary wave solutions from (65)-(66). We see that for the limit where $\xi^2 \gg \eta^2$ (shown in panel (a)), the solutions generally agree with the simplification given in (67)-(68) (a representative of such solutions was shown in panel (a) of Fig. 6). As η increases relative to ξ (still subject to the restriction $0 < |\eta| < |\xi|$), we find that the oscillations within the central wave packet decrease and the filament becomes much more regular in form. These wave packets will propagate along the vortex filament in time, while the constituent oscillations will rotate around the reference axis.

In similar ways, one can use the inverse scattering transform results in the literature to obtain multi-soliton solutions, breathers, and other such solution forms under the WKIS model (10) and then map these into vortex filament solutions under the 2D-LIA. One should then recover the analogues to the LIA solutions derived previously in citations mentioned above. We should note that these results are valid in the very low temperature limit, where mutual friction terms are vanishingly small. In the warmer superfluid case, solitary waves or topological kinks are possible at smaller timescales, before they collapse due to the mutual friction effects. In this way, the mutual friction terms will tend to smooth these solitary structures over time. This was considered in [26, 27].

VI. DISCUSSION

Using the fact that the 2D-LIA can be mapped into the first equation in the WKIS hierarchy, we have been able to use solutions to this WKIS equation in order to construct vortex filament solutions to the 2D-LIA. The 2D-LIA is derived from the Hamiltonian formulation of Svistunov, which itself is valid for a vortex filament in the Cartesian frame aligned along one axis. As such, the 2D-LIA solutions immediately give one a vortex filament in the natural Cartesian space. Therefore, we remark that the approach discussed herein allows one to rather simply recover solutions, and that the solutions obtained are completely relevant to what is seen in actual experimental observations or numerical simulations of low temperature vortex filament dynamics (as discussed in each of the relevant sections). Part of the reason that this approach was successful lies in the fact that the 2D-LIA (8) is a scalar equation. In the warmer-temperature limit, when mutual friction and normal fluid effects are no longer negligible (as in the Schwartz model [35]), the relevant model equation becomes more complicated. In some limits that equation can be put into scalar form

(for weak normal fluid effects [27]), otherwise one must work with some other reduction or the full vector equation. In the case where scalar equations are possible, one can study soliton-like solutions that persist over certain timescales before decaying due to friction effects [26, 27]. For some of the solutions, such as the soliton and planar filaments, the WKIS solutions were already known in the literature and hence were easily mapped into vortex filament solutions under the 2D-LIA, such as the solitary wave solutions. In other cases, such as for the self-similar or stationary solutions, solutions known previously under the 2D-LIA were found easily under the WKIS framework.

One main benefit of the approach used here is that it enables us to obtain the vortex filament curve directly. Usually, one obtains a solution of the NLS equation, which from the Hasimoto map can be put into correspondence with the curvature and torsion of an LIA vortex filament solution. With curvature and torsion known (up to some scaling constants), one integrates the Frenet-Serre formulas in order to obtain the tangent, normal, and bi-normal vectors to the vortex filament curve. After these are found, one finally integrates along the tangent vector to obtain a vortex filament curve. Although one may obtain exact or analytical solutions to the NLS equation, the integration of the Frenet-Serre formulas is often performed numerically, meaning that the resulting vortex filament curve still needs to be obtained numerically. Using the correspondence between the 2D-LIA and the WKIS solutions, we may bypass this more complicated procedure, since we can directly obtain a vortex filament curve from the 2D-LIA once a WKIS solution is known. Furthermore, exact or analytical solutions to the WKIS equation result in exact or analytical vortex filament curves in Cartesian coordinates, since numerical integration of the Frenet-Serre formulas is not needed.

Generalized stationary states were considered in Sec. III, and these solutions consist of vortex filaments which maintain their form as they rotate about a reference axis. What is nice about the approach used here (in particular, the connection between the WKIS and 2D-LIA) is that we are able to obtain nice analytical approximations in (31)-(32). These analytical approximations give us a better understanding of the generalized stationary states previously claimed to exist numerically in [21]. Indeed, from the analytical solutions, we are able to obtain solutions which effectively generalize the helical filaments ore common in the literature. Some of these analytical curves are shown in Fig. 2, and these recover some of the numerical structures observed in [21]. Analytical solutions for these generalized stationary states were not previously found in the literature, yet the WKIS framework has afforded us the chance to obtain such approximate analytical solutions rather easily. Note also that by using the WKIS framework, one may recover planar and helical filaments previously considered in the literature, with minimal effort (and we show this in Sec. III, as well).

From Sec. IV, we now know the type of self-similarity possible under the WKIS model. Self-similarity is a trait shared among many integrable models, and is quite distinct from other common solution forms (such as traveling wave solutions or stationary solutions) in that it yields solutions that appear to have the same structure at various timescales. Due to the form of self-similarity observed, the self-similar solutions to the WKIS equation remain bounded provided that the similarity function itself remains bounded. In contrast, other integrable models can admit similarity solutions that scale as \sqrt{t} or $1/\sqrt{t}$, yielding large or small time blow-up, respectively. In Sec. IV we were able to obtain analytical approximations to the self-similar dynamics of vortex filaments, and these agree with what was shown in [22] through a different approach.

Solitary waves along the vortex filament should be expected to exist for the 2D-LIA reduction of the 3D-LIA model, since related solitons were found theoretically for the standard LIA by way of the Hasimoto transformation and ten years later were found experimentally. However, as explained in [22], such solutions are hard to recover from the 2D-LIA directly. Part of the complication is that the solitary waves (such as those discussed here) really involve two wave variables with differing wave speeds, as the amplitude and phase of the solutions will evolve at different rates (in general). In contrast, it was shown in [22] that traveling wave solutions in one wave variable result in helices. From Sec. V, we find that solitary waves translate along the reference axis, with solutions analogous to 1-solitons consisting of a single wave packet in which the filament curve oscillates. The particular shape of the solitary wave along the vortex filament will depend on two parameters, which act to broaden and increase the twist or torsion on the filament. This can be seen in Fig. 7, where the filament becomes more tightly coiled with a decrease in the shape parameter η . In the case where $\xi^2 \gg \eta^2$, the solitary waves take on a similar appearance to the Hasimoto 1-soliton in Cartesian coordinates. The wave envelope for that case behaves like the integral of a hyperbolic secant (again in agreement with the solution derived from the bright soliton solution for the NLS equations). It should be possible to consider the n -soliton solutions from the WKIS equation in order to construct filament curves which consist of n wave packets translating along the filament curve. The structure of each wave packet will be similar to the single wave packet shown in Fig. 7.

Regarding future work, note that the correspondence between the 2D-LIA and the WKIS equation (10) is rather direct. Somewhat less direct would be a map between the non-local equation for the 2D Biot-Savart dynamics given by the Hamiltonian formulation (4) and a non-local analogue to the WKIS equation (10). Assuming that the relevant non-local WKIS equation was simpler to solve than the 2D Biot-Savart equation (which is certainly possible, considering that the local WKIS equation (10) is simpler to solve than directly solving the 2D-LIA (8)), this may provide a route to obtaining analytical solutions (under some conditions) for the Biot-Savart dynamics. Such dynamics are

much harder to study analytically (hence the common use of the LIA), and any approach that permits one to obtain analytical solutions to these dynamics would be worthy of investigation. Recent work [3] suggests that a Biot-Savart law can be obtained via a NLS equation, and this approach may merit further consideration in the context of the 2D-LIA.

-
- [1] G. Boffetta, A. Celani, D. Dezzani, J. Laurie, and S. Nazarenko, *J. Low Temp. Phys.* 156, 193 (2009).
 - [2] B. Svistunov, *Phys. Rev. B* 52, 3647 (1995).
 - [3] M. D. Bustamante and S. V. Nazarenko, arXiv preprint arXiv:1507.07806 (2015).
 - [4] L. S. Da Rios, *Rend. Circ. Mat. Palermo* 22, 117 (1906).
 - [5] R. J. Arms and F. R. Hama, *Phys. Fluids* 8, 553 (1965).
 - [6] H. Hasimoto, *J. Fluid Mech.* 51, 477 (1972).
 - [7] D. Levi, A. Sym, and S. Wojciechowski, *Physics Letters A* 94(9), 408 (1983).
 - [8] M. Umeki, *Theor. Comput. Fluid Dyn.* 24, 383 (2010).
 - [9] H. Salman, *Phys. Rev. Lett.* 111, 165301 (2013).
 - [10] H. Salman, *Journal of Physics: Conference Series* 544, 012005 (2014).
 - [11] R. L. Ricca, *Chaos* 3, 83 (1993).
 - [12] E. J. Hopfinger and F. K. Browand, *Nature* 295, 393 (1982).
 - [13] E. J. Hopfinger, F. K. Browand, and Y. Gagne, *J. Fluid Mech.* 125, 505 (1982).
 - [14] T. Maxworthy, E. J. Hopfinger, and L. G. Redekopp, *J. Fluid Mech.* 151, 141 (1985).
 - [15] K. Konno, *J. Phys. Soc. Japan* 59, 3417 (1990).
 - [16] K. Konno, M. Mituhashi, and Y. H. Ichikawa, *Chaos, Solitons & Fractals* 1, 55 (1991).
 - [17] K. Konno and Y. H. Ichikawa, *Chaos, Solitons & Fractals* 2, 237 (1992).
 - [18] J. Cieřliński, *Physics Letters A* 171, 323 (1992).
 - [19] M. Wadati, K. Konno, and Y. H. Ichikawa, *J. Phys. Soc. Jpn.* 46, 1965 (1979).
 - [20] T. Shimizu and M. Wadati, *Prog. Theor. Phys.* 63, 808 (1980).
 - [21] R. A. Van Gorder, *Phys. Fluids* 26, 065105 (2014).
 - [22] R. A. Van Gorder, *Phys. Fluids* 27, 095104 (2015).
 - [23] M. Lakshmanan and S. Ganesan, *J. Phys. Soc. Jpn.* 52, 4031 (1983).
 - [24] M. Lakshmanan and S. Ganesan, *Physica A* 132, 117 (1985).
 - [25] M. Boiti, V. S. Gerdjikov, and F. Pempinelli, *Prog. Theor. Phys.* 75, 1111 (1986).
 - [26] R. A. Van Gorder, *J. Fluid Mech.* 740, 5 (2014).
 - [27] R. A. Van Gorder, *Physical Review E* 91, 053201 (2015).
 - [28] R. A. Van Gorder, *Progress of Theoretical Physics* 128, 993 (2012).
 - [29] R. A. Van Gorder, *J. Phys. Soc. Jpn.* 82, 064005 (2013).
 - [30] H. Hasimoto, *J. Phys. Soc. Jpn.* 31, 293 (1971).
 - [31] S. Kida, *J. Fluid Mech.* 112, 397 (1981).
 - [32] S. Kida, *J. Phys. Soc. Jpn.* 51, 1655 (1982).
 - [33] R. A. Van Gorder, *Phys. Rev. E* 86, 057301 (2012).
 - [34] R. A. Van Gorder, *Phys. Rev. E* 87, 043203 (2013).
 - [35] K. W. Schwarz, *Phys. Rev. B* 31, 5782 (1985).
 - [36] R. A. Van Gorder, *Proc. R. Soc. A* 470, 20140341 (2014).
 - [37] E. B. Sonin, *EPL* 97, 46002 (2012).
 - [38] D. K. Cheng, W. M. Cromar, and R. J. Donnelly, *Phys. Rev. Lett.* 31, 433 (1973).
 - [39] W. I. Glaberson, W. W. Johnson, and R. M. Ostermeier, *Phys. Rev. Lett.* 33, 1197 (1974).
 - [40] R. M. Ostermeier and W. I. Glaberson, *J. Low Temp. Phys.* 21, 191 (1975).
 - [41] R. A. Van Gorder, *Phys. Fluids* 26, 075101 (2014).
 - [42] H. U. Quaranta, H. Bolnot, and T. Leweke, *J. Fluid Mech.* 780, 687 (2015).
 - [43] O. V. Fuentes, Motion of a helical vortex. arXiv preprint arXiv:1508.00272 (2015).
 - [44] R. A. Van Gorder, *J. Fluid Mech.* 762, 141 (2015).
 - [45] R. A. Van Gorder, *Proc. R. Soc. A* 471(2179), 20150149 (2015).
 - [46] T. Lipniacki, *Phys. Fluids* 15, 1381 (2003).
 - [47] T. Lipniacki, *T. 2003 J. Fluid Mech.* 477, 321 (2013).
 - [48] R. A. Van Gorder, *Phys. Fluids* 25, 095105 (2013).
 - [49] S. Gutierrez, J. Rivas, and L. Vega, *Commun. in P.D.E.* 28, 927 (2003).
 - [50] V. Banica and L. Vega, *Commun. Math. Phys.* 286, 593 (2009).
 - [51] V. Banica and L. Vega, *J. Eur. Math. Soc.* 14, 209 (2012).
 - [52] S. Gutierrez and L. Vega, *Mathematische Annalen* 356, 259 (2013).
 - [53] M. Kurs, K. Bajer, and T. Lipniacki, *Phys. Rev. B* 83, 014515 (2011).
 - [54] E. Fonda, D. P. Meichle, N. T. Ouellette, S. Hormoz, and D. P. Lathrop, *Proc. Natl. Acad. Sci. USA* 111, 4707 (2014).